Tellus
SERIES A
DYNAMIC
METEOROLOGY
AND OCEANOGRAPHY
PUBLISHED BY THE INTERNATIONAL METEOROLOGICAL INSTITUTE IN STOCKHOLM

Tellus (2010), 62A, 48–61

TELLUS

Can an atmospherically forced ocean model accurately simulate sea surface temperature during ENSO events?

By A. BIROL KARA, HARLEY E. HURLBURT*, CHARLIE N. BARRON, ALAN J. WALLCRAFT and E. JOSEPH METZGER, *Naval Research Laboratory, Oceanography Division, Bldg. 1009, Stennis Space Center, MS 39529, USA*

(Manuscript received 8 April 2009; in final form 22 October 2009)

ABSTRACT

The performance of an atmospherically forced ocean general circulation model (OGCM) in simulating daily and monthly sea surface temperature (SST) is examined during the historical El Niño Southern Oscillation (ENSO) events during the time period 1993–2003. For this purpose, we use the HYbrid Coordinate Ocean Model (HYCOM) configured for the North Pacific north of 20°S at a resolution of ≈9 km. There is no assimilation of (or relaxation to) SST data and no date-specific assimilation of any data type. The ability of the model in simulating temporal variations of SST anomalies is discussed by comparing model results with two satellite-based SST products. The HYCOM simulation gives a basin-averaged monthly mean bias of 0.3 °C and rms difference of 0.6 °C over the North Pacific Ocean during 1993–2003. While the model is able to simulate SST anomalies with mean biases <0.5 °C in comparison to observations during most of the ENSO events, limitations in the accuracy of atmospheric forcing (specifically, net short-wave radiation) have some influence on the accuracy of simulations. This is specifically demonstrated during the 1998 transition period from El Niño to La Niña, when a record large SST drop of ≈7 °C occurred in the eastern equatorial Pacific Ocean.

1. Introduction

Sea surface temperature (SST) is one of the most important characteristics of El Niño Southern Oscillation (ENSO) events, since a marked shift in its anomalies occurs between the warm (El Niño) and cold (La Niña) phases (McPhaden, 1999). In the equatorial Pacific there is an east–west asymmetry where a warm (cold) SST anomaly in the east is associated with a cold (warm) one in the west (Nakajima et al., 2004). In addition, Mitchell and Wallace (1992) demonstrated the asymmetry in interannual variations of SST due to heat flux variations at the surface along with radiative and cloud feedbacks.

The interannual variability in tropical Pacific SST may primarily be linked to ENSO events, but other variations in atmospheric climate also play a role (Enfield, 1996). For example, warmer SSTs typically provide favourable conditions for stronger atmospheric convection, but weaker convection may prevail due to large-scale atmospheric circulation in the tropics (e.g. Lau et al., 1997). Traditionally, it is well known that deep atmospheric convection and heavy rainfall occur in the western Pacific over the warm water, whereas there is net atmospheric subsidence over the colder water in the eastern Pacific. This suggests that under some circumstances, the absence/presence of deep convection is generally associated with SSTs that are colder/warmer than usual. With this range of conditions, ENSO events provide a challenging opportunity to investigate SST variability in relation to atmospheric forcing.

In this paper, the skill of an eddy-resolving ocean model in simulating SST is examined over the period 1993–2003, when several El Niño and La Niña events occurred. In fact, one major focus is to examine the accuracy of SST from the model during the 1997–1998 ENSO event. The 1997 El Niño event developed very rapidly, with a record high SST anomaly occurring in the equatorial Pacific, and was followed by the abrupt 1998 transition to La Niña, which resulted in particularly cold SST values. Because the large variations in strength and evolution of ENSO events make tropical Pacific SST simulation by an OGCM a great challenge on interannual time scales, we will also present model-data comparisons of SST anomalies.

2. Ocean model

The HYbrid Coordinate Ocean Model (HYCOM) is a community ocean model (http://www.hycom.org) and uses a generalized (hybrid isopycnal/terrain-following (σ)/z-level) vertical coordinate (Bleck, 2002). Typically, the vertical coordinate is isopycnal in the stratified ocean, but the model uses the layered continuity equation to make a dynamically smooth transition to

*Corresponding author.
e-mail: hurlburt@nrlssc.navy.mil
DOI: 10.1111/j.1600-0870.2009.00422.x

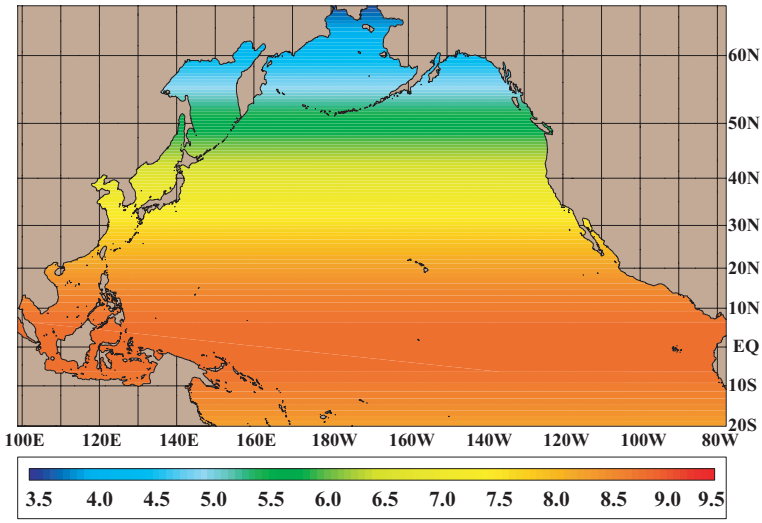

Fig. 1. Grid length (in km) in 0.08° HYCOM as configured for the Pacific Ocean north of 20°S. Latitude and longitude labels in the figure are also used as references for the rest of the figures throughout the paper.

pressure coordinates (approximately fixed-depth z-levels) in the unstratified surface mixed layer or to σ-levels (terrain-following coordinates) in shallow water. The optimal coordinate is chosen every time step using a hybrid coordinate generator. In this way, the model automatically generates the lighter isopycnal layers needed to represent the pycnocline during summer, while the same layers may define a well-mixed zone using z-levels during winter.

2.1. *Pacific HYCOM configuration*

The model domain spans the Pacific Ocean from 20°S to 65°N. Pacific HYCOM is configured at a resolution of 0.08° cos (lat) × 0.08° (latitude × longitude) on a Mercator grid. As seen from Fig. 1, the grid length is ≈9 km at the equator (111 km deg^{-1} × 0.08° = 8.88 km) and ≈7 km [111 km deg^{-1} × 0.08° × cos (40) = 6.8 km] at mid-latitudes (e.g. at 40°N). Zonal and meridional array dimensions for Pacific HYCOM are 2294 and 1362, respectively. Hereinafter the model resolution will be referred to as 0.08° for simplicity.

The model includes 20 hybrid layers in the vertical. The top 10 layers may become z or sigma levels. The layer structure was chosen such that the upper five are typically z-levels to help resolve the mixed layer, but this varies spatially. In general, HYCOM needs fewer vertical coordinate surfaces than say, a conventional z-level model, because isopycnals are more efficient in representing the stratified ocean, as further discussed in Kara et al. (2005a).

2.2. *Atmospheric forcing*

HYCOM uses the following time-varying atmospheric fields to define two types of forcing: wind forcing (zonal and meridional components of wind stress, wind speed at 10 m above the sea surface) and thermal forcing (air temperature and air mixing ratio at 2 m above the sea surface, precipitation, net short-wave radiation and net long-wave radiation at the sea surface). All these climatological monthly mean wind and thermal forcing parameters were formed from the 1.125° × 1.125° ECMWF Re-Analysis (ERA-15) over 1979–1993 (Gibson et al., 1997). For example, the climatological January mean for a given variable is the average of all Januaries from ERA-15 from 1979 to 1993.

In order to be compatible with the interannual simulation with 6-hourly atmospheric forcing, representative 6-hourly intra-monthly anomalies are added to the monthly wind climatologies. This is also necessary because the mixed layer is sensitive to variations in surface forcings on time scales of a day or less (Wallcraft et al., 2003). The 6-hourly anomalies are obtained from a reference year. For that purpose, the winds from September 1994 to September 1995 (6-hourly) are used, inclusive, because they represent a typical annual cycle of the ECMWF winds, and because the September winds in 1994 and 1995 most closely matched each other.

Additional forcing parameters read into the model are monthly mean climatologies of satellite-based attenuation coefficient for photosynthetically active radiation (k_{PAR} in 1 m^{-1}) and river discharge values. The short-wave radiation at depth is calculated using a spatially varying monthly k_{PAR} climatology as processed from the daily-averaged k_{490} (attenuation coefficient at 490 nm) data set from Sea-viewing Wide Field-of-view Sensor (SeaWiFS) spanning 1997–2001. This ocean colour data allows the effects of water turbidity to be included in the model simulations through the attenuation depth ($1/k_{\mathrm{PAR}}$) for the short-wave radiation. The rate of heating/cooling of model layers in the upper ocean is obtained from the net heat flux absorbed from the sea surface down to the depth of solar penetration, including water turbidity effects (Kara et al., 2005a).

The model treats rivers as a runoff addition to the surface precipitation field. The freshwater influx is first applied to a single ocean grid point and smoothed over surrounding ocean

grid points, yielding a contribution to precipitation in $m\,s^{-1}$. This works independently of any other surface salinity forcing. Monthly mean river discharge values were constructed at NRL (Barron and Smedstad, 2002). This river data set comes from Perry et al. (1996), which had one annual mean value for each river, but the set was converted to monthly values using other data sources for use in ocean modelling studies.

Latent and sensible heat fluxes at the air–sea interface are not taken directly from ECMWF due to their uncertainties. They are calculated using the model's top layer (top 3 m) temperature at each model time step with efficient and computationally inexpensive bulk formulas, whose exchange coefficients are expressed as polynomial functions of air–sea temperature difference, air–sea mixing ratio difference, and wind speed at 10 m to parametrize stability (Kara et al., 2000a). Including air temperature and model SST in the formulations for latent and sensible heat flux automatically provides a physically realistic tendency towards the correct SST in the model simulations (Kara et al., 2003; Wallcraft et al., 2003). The radiation flux (net short-wave and net long-wave fluxes at the sea surface) depends on cloudiness and is taken directly from ECMWF for use in the model.

2.3. Model simulations

The model simulations were performed with no assimilation of any oceanic data. There was only weak relaxation to sea surface salinity to keep the salinity budget in balance in the model. We used realistic bottom topography constructed by merging the Earth Topography Five Minute Grid (ETOP05) and Smith and Sandwell (1997) with numerous hand edits. The model was initialized from the Generalized Digital Environmental Model (GDEM) climatology of the U.S. Navy at 1/4° resolution (Carnes, 2009).

After an initial 8 yr HYCOM run with purely climatological forcing, the simulation was continued at 0.08° resolution until it reached near statistical equilibrium (about 28 yr) using climatological monthly mean thermal atmospheric forcing, but with wind forcing that includes the 6-hourly variability (Kara et al., 2005b). After the spin-up, the climatologically forced Pacific simulation was extended interannually using 6-hourly wind and thermal forcing from ERA-15 (1979–1993) and then continued using ECMWF operational data (1994–2003). The K-Profile Parametrization (KPP) mixed layer model (Large et al., 1994) is used in the model simulation. Mixed layer depth in the model can be computed following Kara et al. (2000b). Performing a 1-month simulation took ≈18 wall-clock hours on 297 IBM SP POWER3 processors.

3. Climatological SST in the Pacific Ocean

We first examine the accuracy of SSTs obtained from the climatologically forced HYCOM simulation. Since our focus is on SST, monthly mean SST from the model is validated against satellite-based Pathfinder and Modular Ocean Data Analysis System (MODAS) SST climatologies. The use of two different data sets for HYCOM validation will help to indicate whether or not the deficiencies of model simulations in certain regions, such as the equatorial Pacific Ocean and the ice-free high northern latitudes, are due to model error or to the validation data set used. The dual validation will also better determine the accuracy of model results. A brief explanation of both data sets is given along with the statistical metrics used for the model validation.

The Pathfinder climatology is an update of Casey and Cornillon (1999) and is generated using the same techniques (K. Casey, 2008, personal communication). It has finer spatial resolution than the previous version (4 km rather than 9 km) and an improved land mask, which allows for more retrievals along coastlines and in lakes. The monthly climatology covers 1985–2001, as directly provided by the originator. This climatology does not take the existence of ice into account (i.e. treats it as a data void). Thus, we added the National Oceanic and Atmospheric Administration (NOAA) ice climatology (Reynolds et al., 2002) to the Pathfinder SST climatology. This is done for each month using a monthly mean ice climatology. Ice-free regions are then determined based on the ice-land mask from the NOAA climatology over the global ocean.

Similarly, the monthly mean MODAS SST climatology is based on Advanced Very-High Resolution Radiometer (AVHRR) Multi-Channel SST (MCSST), as described in Barron and Kara (2006). MODAS SST data are available at http://www7320.nrlssc.navy.mil/modas2d. It gives accurate SSTs with very small rms errors of $< 0.4°$ in comparison to the SST time series from moored buoys over the global ocean (Kara and Barron, 2007). Mean SST for each month is obtained using daily SSTs during 1993–2003. The mean January SST climatology is formed using monthly January SSTs over 11 yr, and the same process is repeated for other months to construct the mean MODAS climatology. Both the Pathfinder and MODAS climatologies are interpolated to the Pacific HYCOM grid for comparisons with the model SSTs.

3.1. Statistical metrics

For comparisons with the Pathfinder and MODAS climatologies, monthly mean HYCOM SST climatologies are constructed using daily model SST output from the climatologically forced simulation. The model output was archived as a daily snapshot rather than a daily mean. Monthly means were formed using daily snapshots. The relatively long (7-yr) time series helps to average out the strong non-deterministic component due to mesoscale flow instabilities that develop in some regions of HYCOM with 0.08° resolution. Monthly mean HYCOM SST fields are then compared to the Pathfinder and MODAS climatologies at each model grid point over the model domain.

The set of statistical metrics used for the model SST validation procedure includes mean error (ME), root-mean-square (rms) SST difference, correlation coefficient (R), conditional bias (B_{cond}), unconditional bias (B_{uncond}) and non-dimensional skill score (SS). Let $X_i (i = 1, 2, \cdots, 12)$ be the set of monthly mean MODAS (or Pathfinder) reference (observed) SST values from January to December, and let $Y_i (i = 1, 2, \cdots, 12)$ be the set of corresponding HYCOM estimates at each model grid point. Also let $\overline{X}(\overline{Y})$ and $\sigma_X(\sigma_Y)$ be the mean and standard deviations of the reference (estimated) values, respectively. The statistical metrics (Murphy, 1995) between MODAS (or Pathfinder) and HYCOM SST time series at a given grid point are expressed as follows:

$$\text{ME} = \overline{Y} - \overline{X}, \tag{1}$$

$$\text{rms} = \left[\frac{1}{n}\sum_{i=1}^{n}(Y_i - X_i)^2\right]^{1/2}, \tag{2}$$

$$R = \frac{1}{n}\sum_{i=1}^{n}(X_i - \overline{X})(Y_i - \overline{Y})/(\sigma_X \sigma_Y), \tag{3}$$

$$\text{SS} = R^2 - \underbrace{[R - (\sigma_Y/\sigma_X)]^2}_{B_{\text{cond}}} - \underbrace{[(\overline{Y} - \overline{X})/\sigma_X]^2}_{B_{\text{uncond}}}. \tag{4}$$

We evaluate SST time series between HYCOM and MODAS (or Pathfinder) over the seasonal cycle, so n is 12 at a given grid point. The non-dimensional metric (SS) takes both conditional bias (the one due to differences in standard deviations) and unconditional bias (the one due to differences in means) into account between the two time series. SS is 1.0 for perfect HYCOM SST simulations and negative for poor model simulations.

3.2. Climatological SST error statistics for HYCOM

Figure 2 shows results of statistical comparisons of the HYCOM SST climatology to the MODAS and Pathfinder SST climatologies. In particular, for the given atmospheric wind and thermal forcing from ECMWF, the annual mean error map demonstrates that the atmospherically forced HYCOM is able to simulate SST with small errors (within $\pm 0.5\,^{\circ}$C) over most of the Pacific Ocean. Cold model SST biases are in blue and warm SST biases are in red. Overall, SST biases (i.e. HYCOM-MODAS and HYCOM-Pathfinder) are almost the same regardless of the climatology used for validating the model, except that there are some differences at high latitudes (Fig. 3).

Relatively large errors between HYCOM and MODAS SST are more evident than between HYCOM and Pathfinder SST at these high latitude belts. The reason is that the MODAS climatology lacks a realistic ice field, resulting in warmer SST than HYCOM by $>2\,^{\circ}$C. On the contrary, when HYCOM is compared to the Pathfinder climatology, the same biases are largely reduced because we added a realistic ice climatology to the Pathfinder climatology. In particular, the SST includes the ice concentration climatology from NOAA to decide if a data void should be treated as ice. We did not add an ice field to MODAS at high latitudes to demonstrate the differences in the model SST evaluation procedure at high latitudes when using the two climatologies.

The 0.08° resolution HYCOM generally gives a small rms SST difference of $\approx 0.7\,^{\circ}$C calculated over the seasonal cycle (Fig. 3). In fact, the basin-wide areal-average of rms SST difference is $0.71\,^{\circ}$C ($0.72\,^{\circ}$C) when the climatologically forced HYCOM simulation is validated against MODAS (Pathfinder) SST climatology. The rms SST difference is usually small near the equatorial regions and large north of 40°N. However, the model has low skill at the equator and high skill north of 40°N as seen from Fig. 3. The reason is that the amplitude of the seasonal cycle of SST is quite different in the two regions (much smaller in the tropics), so a non-dimensional metric is required to better evaluate model skill in simulating the mean and seasonal cycle of SST (see also the results for R, correlation coefficient).

Biases are taken into account in the rms differences, but in some cases the latter can be small when skill and correlation are poor. This can occur where the amplitude of the seasonal cycle is small, giving a small rms SST difference but also low skill, as in the western equatorial Pacific warm pool (Fig. 2). Near the equatorial Pacific the biases between HYCOM and MODAS (or Pathfinder) SST time series over the seasonal cycle are due mostly to differences in the mean (i.e. large unconditional bias). There is also no model skill in simulating SST in the eastern equatorial Pacific. In particular, the model has a significant warm bias in the cold tongue. This is in contrast to many other OGCMs that suffer from a cold bias.

Obviously, the choice of SST products used for model validation can somewhat alter statistical results. For example, both the Pathfinder and MODAS SST climatologies are satellite-based, and one could ask whether or not the validation results would be significantly different if an alternative data set based on in situ data where used. For this purpose, we interpolate 1° resolution monthly SST climatologies from the World Ocean Atlas 2005 (WOA05) and compare them to the Pathfinder and MODAS climatologies. The WOA05 data set is constructed from in situ observational SSTs only, as described in Locarnini et al. (2005), in detail. Observational data used in this climatology were averaged on $1^{\circ} \times 1^{\circ}$ grids for input to the objective analysis (Boyer et al., 2006). The initial objective analyses usually contained some large-scale gradients over a small area and some bulls eyes. The WOA05 climatology is much coarser than the Pathfinder (almost 0.04°) and MODAS (0.125°) climatologies, but include SSTs from many different sources.

As evident from Fig. 4 , there is very close agreement between the satellite-based SST climatologies and the observation-based WOA05 climatology in the Pacific Ocean north of 20°S. Basin averaged mean SST difference is almost zero ($0.07\,^{\circ}$C) for

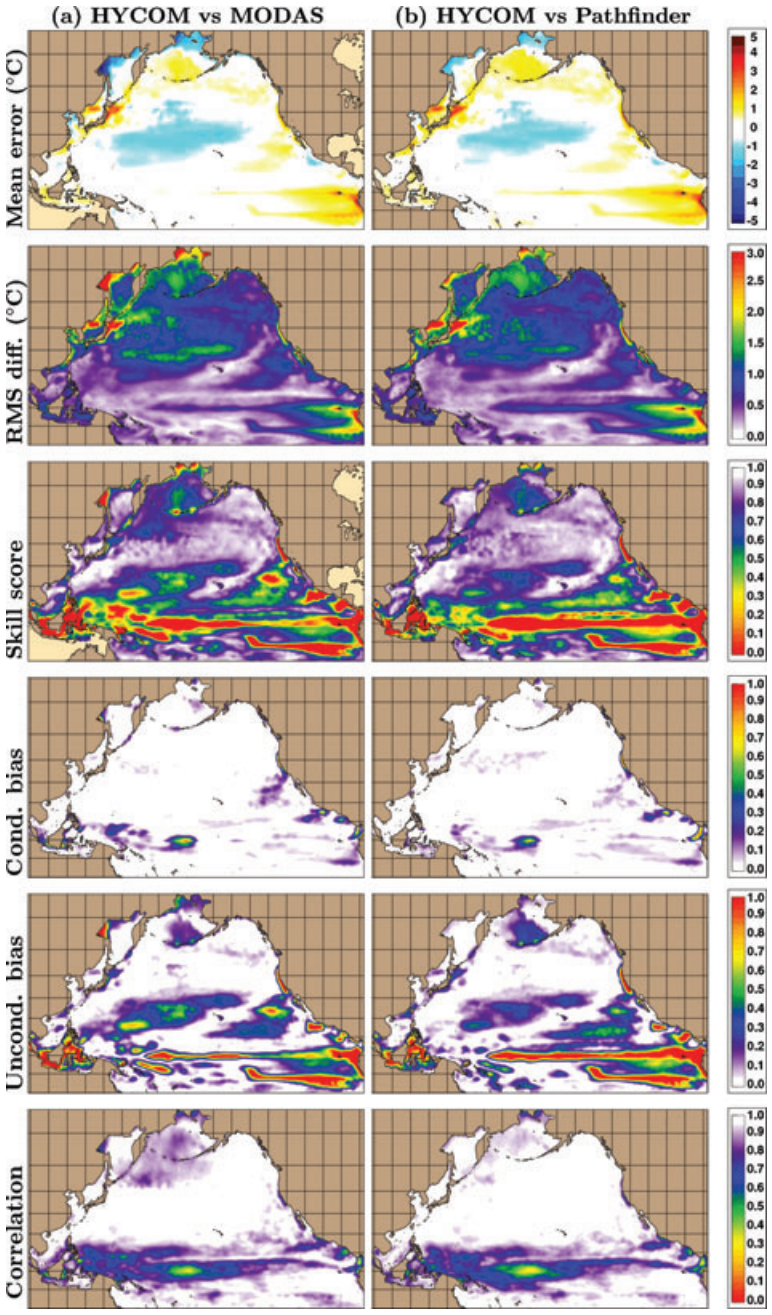

Fig. 2. Statistical validation maps for the climatologically forced HYCOM SST in comparison to two climatological data sets: (a) MODAS and (b) Pathfinder. The mean SST error is computed as follows: HYCOM-MODAS and HYCOM-Pathfinder.

Pathfinder-WOA05 and 0.18 °C for MODAS-WOA05. While plots are not shown, computations over the seasonal cycle reveal basin-wide areal-average rms values of 0.36 and 0.40 °C, respectively. Correlation values are 0.96 and 0.94, again indicating a strong relationship over the seasonal cycle. The skill scores are also very high, close to the perfect skill (i.e. 1.0), with values of 0.84 and 0.79, further indicating the good agreement in comparison to the WOA05 climatology. Moreover, examining a total of six SST climatologies in the tropical Pacific Ocean, Kara, et al. (2009a) demonstrated that all the products including satellite- and observation-based are in good agreement with each other, with basin-averaged mean bias values of almost zero and rms SST differences typically <0.3 °C over the seasonal cycle. For this reason, we limited our choice of data sets in evaluating model results to only two products, Pathfinder and MODAS. As noted above, these two products have relatively fine spatial resolutions, which are the most consistent with the resolution of eddy-resolving HYCOM.

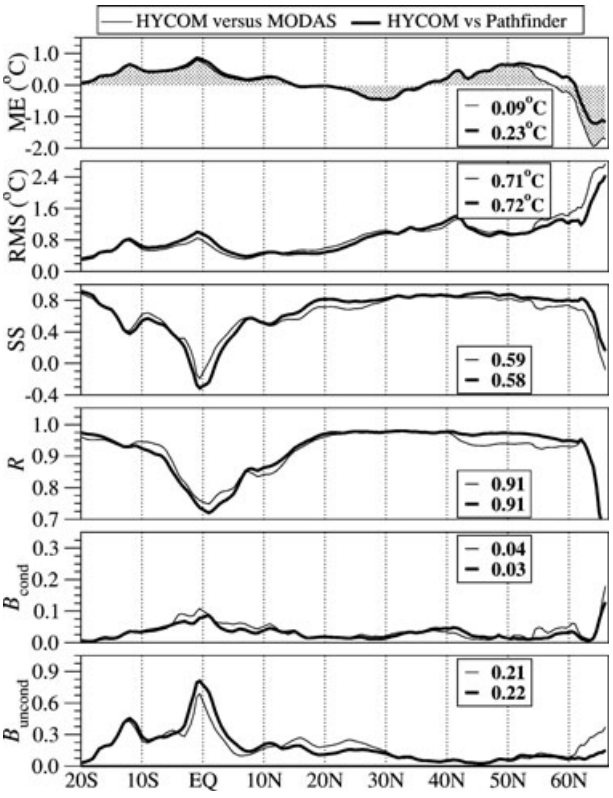

Fig. 3. Zonal averages of statistical maps shown in Fig. 2. The zonal averaging is performed at each 1° latitude belt over the Pacific Ocean north of 20°S. Legends in each panel give the areal-average of statistical metrics when HYCOM SST is evaluated against the MODAS and Pathfinder climatologies.

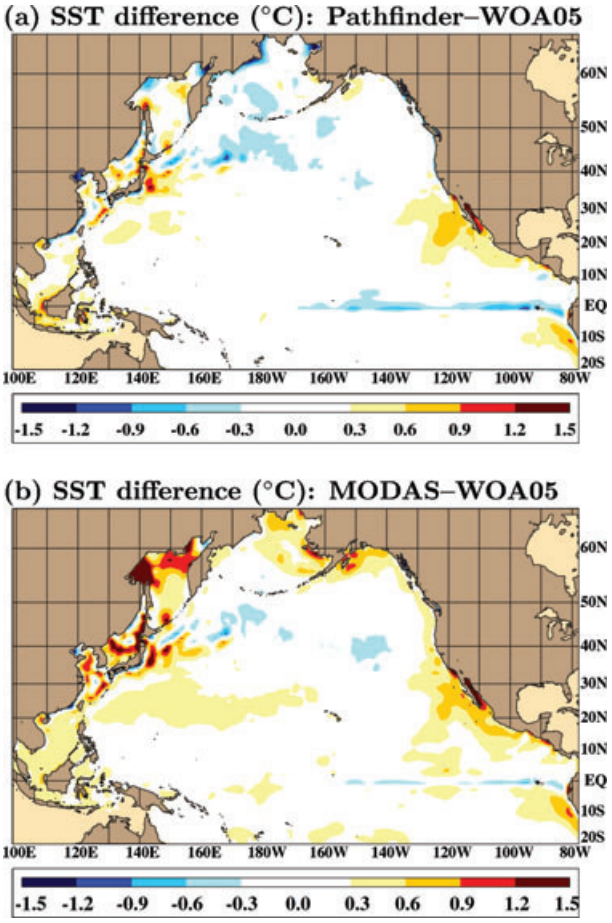

Fig. 4. Annual mean SST difference of the Pathfinder and MODAS climatologies with respect to the WOA05 climatology: (a) Pathfinder-WOA05 and (b) MODAS-WOA05.

4. HYCOM SST validation during 1993–2003

4.1. The 1998 ENSO transition

Earlier studies have indicated that the 1997 El Niño event was transitioning to the 1998 La Niña by early summer 1998 (e.g. Behrenfeld et al., 2001; Nagura et al., 2008). In particular, based on various indices it was identified that the transition occurred from May to August 1998 (Kara et al., 2008). Thus, we first examine the performance of HYCOM in simulating SST in 1998, including the transition period.

Monthly mean SSTs from the model are compared to those from the satellite-based MODAS analysis in the tropical Pacific Ocean spanning the latitudes 20°S–20°N in 1998 (Fig. 5). Patterns of SST from MODAS and HYCOM reveal distinct similarities in the tropical Pacific for each month, and the extent of cold SSTs are nearly identical in the eastern equatorial Pacific after August 1998 (Figs. 5a and b). However, there are also some differences between the two. In particular, SSTs from HYCOM are typically colder (warmer) by $\approx 0.5^{\circ}$ than those from MODAS in the western (eastern) tropical Pacific (Fig. 5c). Warm HYCOM SST biases ($>1.0\,^{\circ}$C) exist in the eastern equatorial Pacific during the ENSO transition period from May to August, and after the beginning of the La Niña, become large within the cold tongue region. Most of these biases can be attributed to the insufficient upwelling in the model (Kara et al., 2008) and to errors in the atmospheric forcing, as will be discussed later.

To construct anomaly fields, mean SST from MODAS and HYCOM are obtained for each month from 1993 to 2003, and the long-term mean (climatology) is formed. For example, using SSTs in January from each year, the mean January SST climatology is first constructed over 11 yr. Finally, the climatological SST in January is subtracted from the January SST field for each year. The same process is repeated for other months.

In general, HYCOM is able to reproduce the extent and magnitude of monthly mean warm (cold) SST anomalies reasonably well during the 1998 transition (Fig. 6). While spatial patterns of the anomalies from MODAS and HYCOM are remarkably similar over the entire region, the SST anomaly from HYCOM is $>1\,^{\circ}$C warmer than that from MODAS in the cold tongue during June 1998, the beginning of the 1998 La Niña. Error

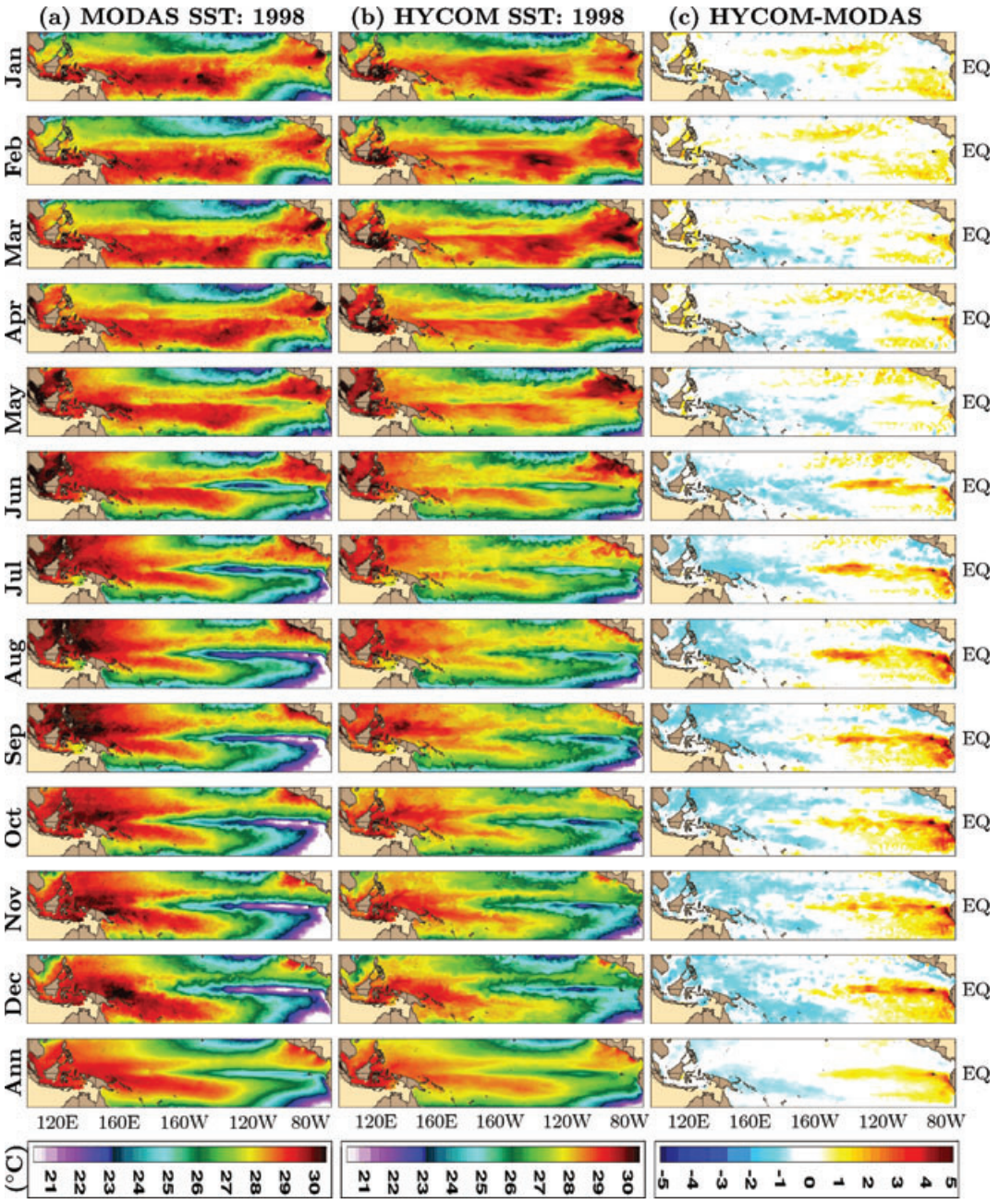

Fig. 5. Spatial variations of monthly SSTs in the tropical Pacific Ocean within 20°S–20°N in 1998: (a) MODAS and (b) HYCOM. Also shown in (c) are differences between the two.

statistics between HYCOM and MODAS are calculated over the time period 1993–2003. This is done for actual SSTs and SST anomalies, separately. While rms values and standard deviations are similar for both actual SST and SST anomalies over the entire region (Figs. 7a and b), there are large differences in the eastern tropical Pacific.

Major differences arise in the conditional biases and correlations (Figs. 7c and d). SST anomaly fields from HYCOM yield relatively large conditional biases and small correlations in comparison to actual HYCOM SSTs when both are validated against MODAS. Large conditional biases for the SST anomalies indicate that differences between MODAS and HYCOM are due largely to the differences in standard deviations between the two since the unconditional bias fields are generally identical (not shown). While the standard deviations for actual SSTs and anomalies differ slightly in the cold tongue (Fig. 7b), this is not reflected in the conditional bias since the differences are small. Relatively lower correlations for the SST anomalies are

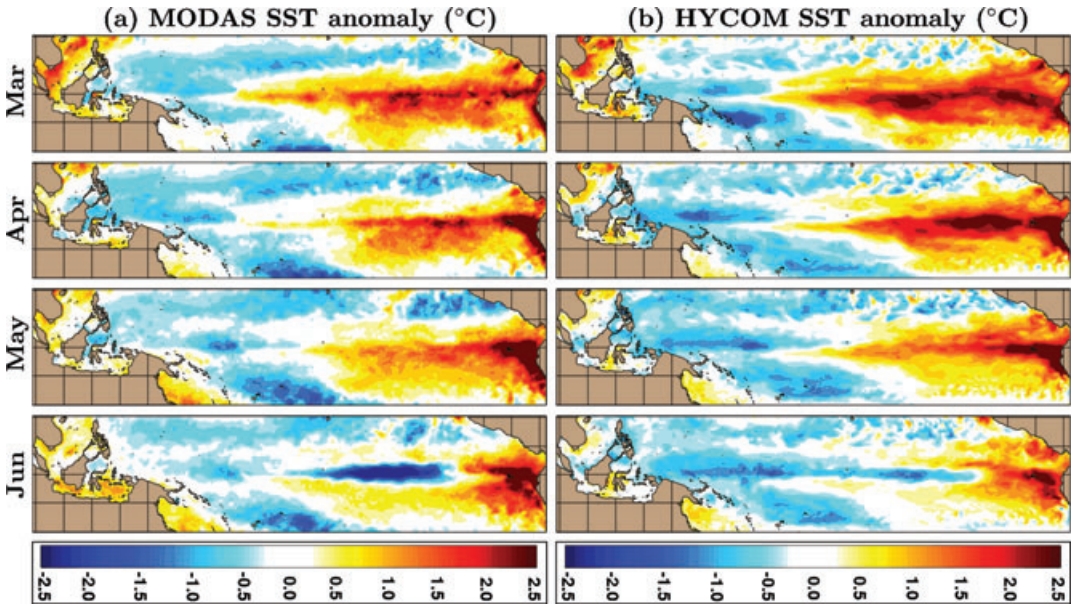

Fig. 6. Monthly mean SST (°C) anomaly fields from MODAS and HYCOM in the tropical Pacific just before, during and after the 1998 transition period from El Niño to La Niña between 20°S and 20°N.

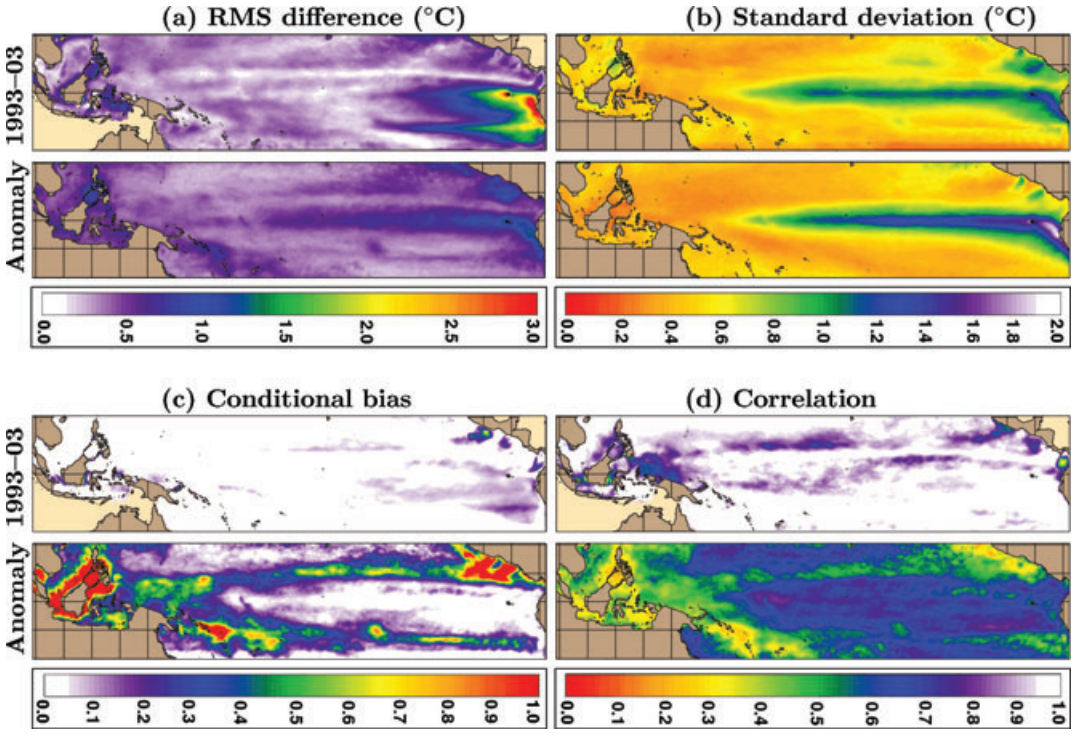

Fig. 7. Statistics between HYCOM and MODAS SST calculated using actual SST (upper panels) and SST anomalies (lower panels), both of which span 1993–2003. In Fig. 7b, the top (bottom) panel shows SST standard deviations of HYCOM (MODAS).

indications of a poor seasonal cycle in HYCOM compared to MODAS. In general, the model performance in simulating SST anomalies is worse than that in simulating the actual SSTs in terms of conditional bias and correlation (Fig. 7). The standard deviation of the actual SSTs over this region is larger than that of the SST anomalies because of the contributions from the spatial variability of the mean and the spatial and temporal variability of the seasonal cycle.

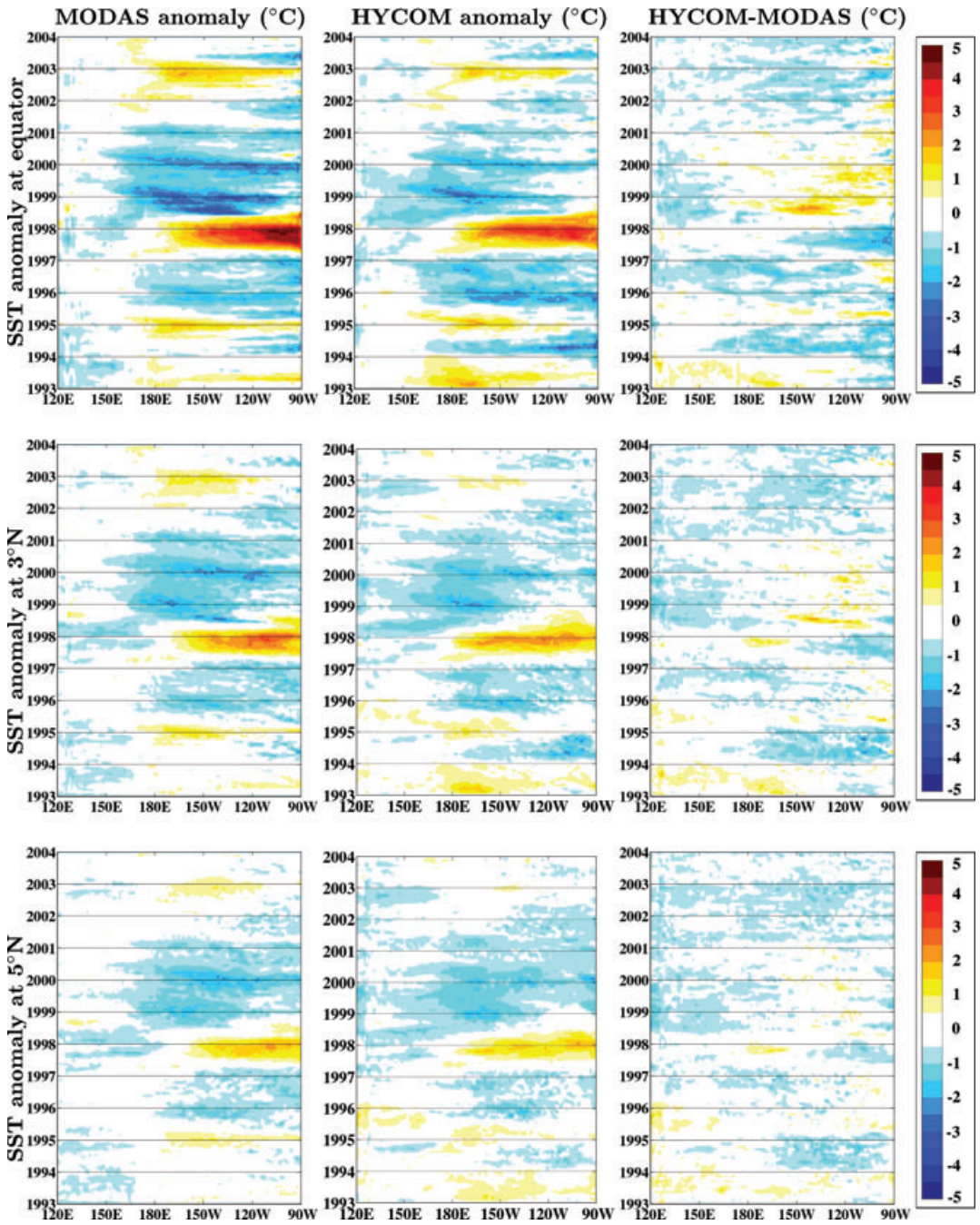

Fig. 8. SST anomalies along the equator, 3°N and 5°N (from top to bottom) in the tropical Pacific Ocean: (a) MODAS and (b) HYCOM. Differences in SST anomalies between HYCOM and MODAS (HYCOM-MODAS) are given in panel (c).

4.2. SST and subsurface temperature anomalies

To further investigate the accuracy of the model results, spatial variations of SST anomalies are investigated not only during the 1998 transition period but also for all years from 1993 to 2003. In addition to SST anomalies, variations in subsurface temperatures are explored. Our purpose is to determine the overall success or failure of the model in simulating temperature anomalies during all strong/weak El Niño, La Niña and neutral events. Based on the Japan Meteorological Index (Hanley et al., 2003), we identified 37 El Niño, 24 La Niña and 71 neutral months during 1993–2003.

Monthly SST anomalies from MODAS and HYCOM reveal similar values as evident along the equator, north of the equator along 3°N and along 5°N (Figs. 8a and b). Relatively large warm SST anomalies during the strongest 1997–1998 ENSO are

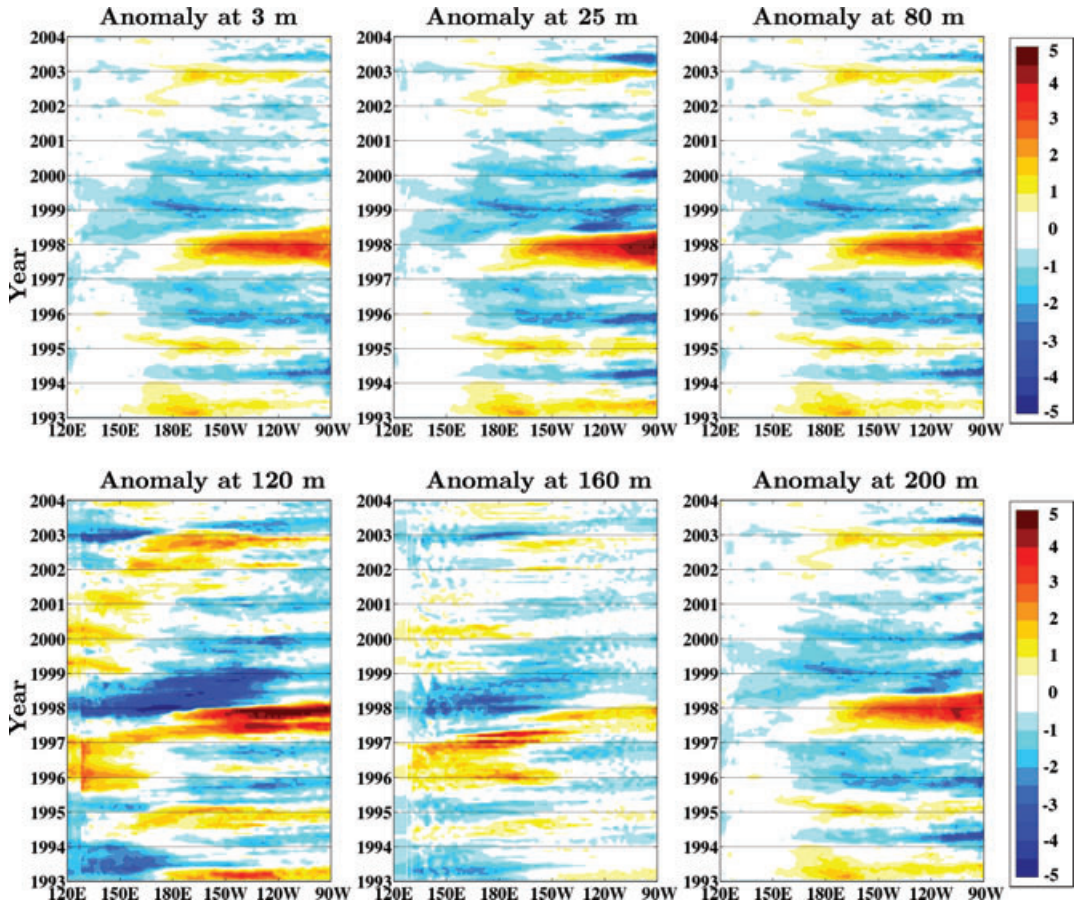

Fig. 9. Subsurface temperature anomalies at various depths. Anomalies are computed at the equator during 1993–2003.

evident from MODAS and HYCOM. Monthly SST anomalies reached a peak ($>2\,^{\circ}$C) at the end of the 1997 El Niño and during the 1998 transition period from El Niño to La Niña between 90°W and 170°W. Similarly, large SST anomalies exist in the same region at 3°N and at 5°N, but they are much smaller ($\approx 1\,^{\circ}$C) in comparison to those at the equator.

While the extent and magnitude of the SST anomalies from HYCOM are similar to those from the satellite-based MODAS product during the 1997–1998 ENSO event, HYCOM has a cold SST bias $>1.0^{\circ}$ between 90°W and 120°W along the equator (Fig. 8c). This bias nearly disappears at 3°N and at 5°N, not only in the eastern equatorial Pacific but also in the western equatorial Pacific. Away from the equator, biases in SST anomalies from HYCOM are generally much smaller (generally within $0.5\,^{\circ}$C).

Using the HYCOM simulation, vertical structure of subsurface temperature anomalies from HYCOM is also examined in the tropical Pacific. Figure 9 shows temperature anomalies at various water depths of 3, 25, 80, 120, 160 and 200 m in the equatorial Pacific. Large temperature anomalies in the eastern and central equatorial Pacific during the 1997–1998 ENSO event, as noted previously (see Fig. 8), are also evident from the subsurface temperature fields. In particular, the existence of relatively warm temperature anomalies extends down to 140 m depth. Temperature anomalies are generally small (within $\pm 1\,^{\circ}$C) for time periods other than the 1997–1998 ENSO event. Cold temperature anomalies strengthen at 60 m across the equatorial Pacific during the 1998 La Niña event, and diminish at 160 m.

4.3. SST and atmospheric forcing

The ocean model used in this study (i.e. HYCOM) typically has a warm bias in simulating SST in the equatorial Pacific during the 1998 transition period from El Niño to La Niña, as presented in the earlier sections. Here, we explore contributions to those biases from atmospheric forcing variables. Additional factors, such as physical parametrizations, mixing schemes in the model, etc., can also contribute to model bias, but here we only focus on a contribution from the surface forcing used in the model simulation, specifically net short-wave radiation at the sea surface, which is one of the most important variables that drives the seasonal cycle of SST from the ocean model (Kara et al., 2009b).

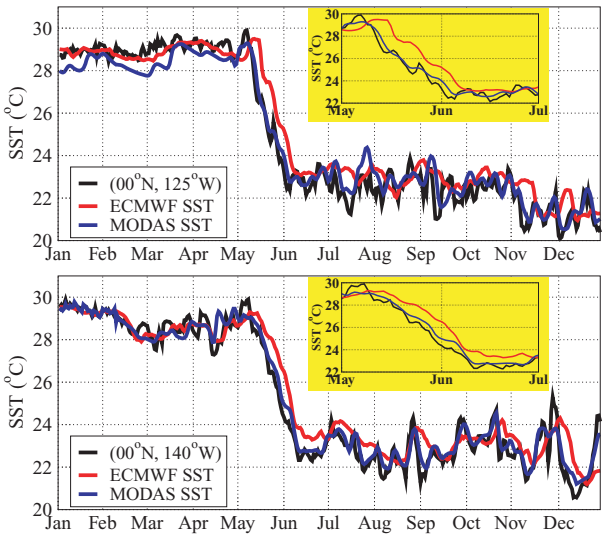

Fig. 10. Daily averaged SST (°C) from two TAO buoys at (0° N, 125° W) and (0° N, 140° W) in the eastern equatorial Pacific during 1998. The *x*-axis is labelled starting from the beginning of each month.

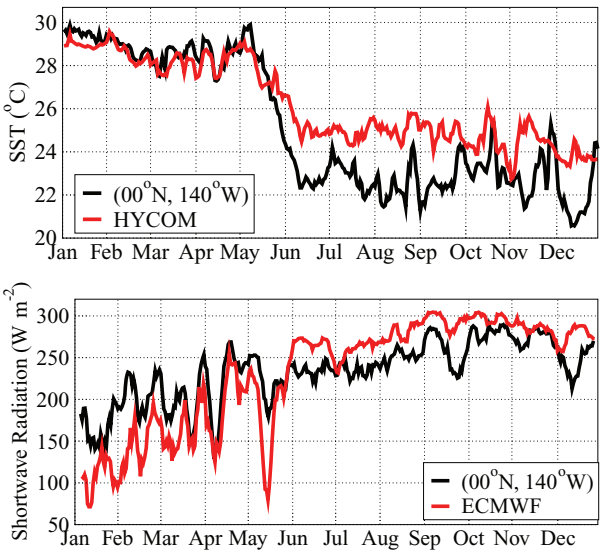

Fig. 11. Time series of daily averaged SST (°C) (from the TAO buoy and HYCOM) and net short-wave radiation (W m^{-2}) at the sea surface (from the TAO buoy and ECMWF) at (0° N 140° W).

Simulating SST from an ocean model is particularly challenging during the 1998 ENSO transition period because of the exceptionally large temperature drop of almost 7 °C in just one month, from May to June. This is clearly evident in daily SSTs obtained from the two Tropical Atmosphere-Ocean (TAO) buoys moored in the eastern equatorial Pacific (Fig. 10). The yellow insets inside each panel show daily SST time series more clearly during May–June 1998. An assessment of instrumental accuracies indicates errors of about 0.02 °C for TAO SST (http://www.pmel.noaa.gov/tao). Also included in Fig. 10 are the daily-averaged SSTs from the ECMWF operational product and the MODAS SST re-analyses, both of which have close agreement with buoy SSTs and confirm the large SST drop during the transition period. Note that the MODAS SST is derived entirely from satellite AVHRR, and thus does not include the TAO data.

Since the large SST drop of ≈7 °C occurred in just a short time period (a month or so), we analyse SST variations during the transition period on daily rather than monthly intervals. Figure 11 shows time series of daily averaged SST and short-wave radiation at (0° N, 140° W). Daily SSTs from HYCOM and daily short-wave radiation from ECMWF, which is used in forcing the model, are compared to observed values of SST and short-wave radiation obtained from the TAO array. Because daily short-wave radiation values are not available at (0° N 110° W), that location is not used in the analyses. As reported from TAO, daily average short-wave radiation is computed as a 24 h average, including day and night time values. It is measured at a height of 3.5 m above mean sea level. Accuracy of the short-wave radiation is ± 2% (http://www.pmel.noaa.gov/tao). Note

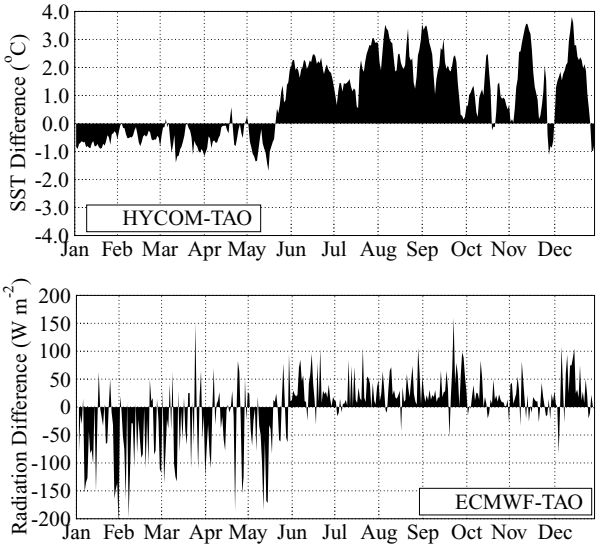

Fig. 12. Differences in SST and short-wave radiation shown in Fig. 11. The annual mean of short-wave radiation from TAO (ECMWF) is 233 (231) W m^{-2}, but note that there are obvious differences between the two on monthly time scales.

that the TAO buoy measures short-wave radiation above the sea surface, and it is multiplied by 0.94 (albedo of sea water) to be consistent with the short-wave radiation from ECMWF. A 7-d running average is applied to the daily short-wave radiation time series for illustration purposes.

Figure 12 shows that a relatively warm model bias (≈ 2 °C) does exist in the daily SST time series at TAO buoy locations (illustrated at (0° N , 140° W)) during the 1998 transition period.

Daily averaged air temperature, wind speed and air mixing ratio from ECMWF are compared to those from TAO buoys at several locations in the eastern equatorial Pacific. They generally agreed within reasonable accuracies (not shown). Thus, here, we also investigate the influence of short-wave radiation errors from the forcing on the SST errors.

In an earlier global study over the annual cycle by Kara et al. (2009c), it was demonstrated that $\approx 100\,\mathrm{W\,m^{-2}}$ difference between annual and monthly mean short-wave radiation is needed to obtain a 1 °C SST change (annual–monthly) in the tropical Pacific where the buoy of interest is located. Based on the values shown in Fig. 12, we computed means of SST differences and short-wave radiation differences. Just before the ENSO transition started in 1998, there was $42\,\mathrm{W\,m^{-2}}$ short-wave radiation difference, consistent with the 0.3 °C SST bias between the model and buoy. However, during the transition period spanning the end of April–June, the $23\,\mathrm{W\,m^{-2}}$ short-wave radiation difference (ECMWF-buoy) explains only a small part of the 1.1 °C SST bias seen during this time. Although the temporal resolution of the SST and forcing data (monthly) in Kara et al. (2009c) is different from that used here (daily), it is obvious that the short-wave radiation errors during the transition period contributed significantly to the SST biases.

The net short-wave radiation from ECMWF does appear to be one contributing reason that the HYCOM SST did not get as cold as the MODAS SST, since there are significant differences in net short-wave radiation between the buoy and ECMWF values, and that would support this hypothesis (Fig. 12). Differences in short-wave radiation between the TAO buoy and ECMWF can even be $>\approx 150\,\mathrm{W\,m^2}$ on daily time scales. The difference was close to $\approx 200\,\mathrm{W\,m^{-2}}$ during mid-May when the 1998 transition just started.

Finally, Fig. 6 revealed that the HYCOM SST anomaly is ≈0.5 °C warmer than MODAS in May and June 1998 at this particular location. A striking feature evident from Fig. 12 is that the short-wave radiation from ECMWF is generally underestimated (overestimated) in the first (second) part of 1998, and some of the errors are likely due to errors in cloudiness. Previously, in another study, Allan et al. (2004) also concluded that in OGCM simulations the accuracy of the solar radiation fields used in the atmospheric forcing can be adversely impacted by errors in representing the extensive equatorial cloudiness. It is noted that other aspects related to the model itself may also contribute errors. For example, insufficient upwelling from the model can clearly reduce the accuracy of SST simulations.

5. Conclusions

This paper demonstrates how an atmospherically forced OGCM (without two-way coupling) may play an important role in representing the ocean component of the climate system on a wide variety of temporal and spatial scales. The daily and monthly SST results were obtained from the model simulation performed with no assimilation of ocean data, and no relaxation to an SST climatology. Results reveal that it is possible to obtain accurate SST with the use of available atmospheric forcing (e.g. ECMWF) for an OGCM (e.g. HYCOM). These accuracies are essential prerequisites for SST assimilation and forecasting using the model. The predictive ability of HYCOM in simulating SST anomalies and the role of uncertainties in the atmospheric forcing were also examined. Solar radiation fields from ECMWF may have serious problems due to the cloudiness, hampering the simulation skill of HYCOM. In this paper, we placed emphasis on the short-wave radiation, and analysed its impact on SST simulation during the 1998 transition from El Niño to La Niña in the eastern and central equatorial Pacific.

Evaluation of HYCOM's ability to simulate SST is one component of the broader model validation that demonstrates its effectiveness as an accurate and generalized ocean model capability. The model is designed to be applicable in a variety of global, regional and littoral applications. HYCOM has additionally been implemented as a global model and global ocean prediction system that can provide boundary conditions to nested models (Hurlburt et al., 2008; Chassignet et al., 2009). Output from the eddy-resolving Pacific HYCOM, as presented here, is made available to users of interest for many types of applications. By understanding the skill of atmospherically forced HYCOM in representing upper ocean variables, users can have greater confidence, for example, in the SST hindcasts and forecasts in assimilative HYCOM implementations.

Uncertainties in the accuracies of cloud cover have been identified as a potentially important source of model error in simulations of SST. Comparisons at a particular TAO buoy location on the equator at 140° W reveals that inaccuracies in short-wave radiation can limit SST accuracy from the model by 1– 2 °C. However, other aspects such as the representation of mixing and dynamics in the ocean model can also contribute. Since SST modifies the net heat flux at the sea surface from the ocean to the atmosphere, two-way coupling of the atmospheric component to an ocean model with skill in simulating SST should lead to more accurate atmospheric predictions. In turn, if these more accurate atmospheric simulations include more accurate cloud cover, the heat flux from the atmosphere to the ocean will allow more accurate simulations of SST.

6. Acknowledgments

We would like to thank two anonymous reviewers for their comments. M. McPhaden of the TAO project office is appreciated for continuous high resolution data support. We would like to thank Ms. J. Dastugue of NRL for processing some of the satellite-based MODAS SST fields. This work was funded by the Office of Naval Research (ONR) as part of the NRL 6.1 project, Global Remote Littoral Forcing via Deep Water

Pathways. The HYCOM simulations were performed on a IBM SP POWER3 at the Army Research Laboratory, Aberdeen, Maryland and on a SGI Origin 3900 at the Aeronautical Systems Center, Wright-Patterson Air Force Base, Ohio, using grants of high performance computer time from the Department of Defense High Performance Computing Modernization Program. The co-authors are sad to report that the lead author, A. Birol Kara, passed away on 14 September 2009 at age 39, after battling cancer for a year and a half. This is contribution NRL/JA/7320/09/9192 and has been approved for public release.

References

Allan, R. P., Ringer, M. A., Pamment, J. A. and Slingo, A. 2004. Simulation of the Earth's radiation budget by the European Centre for Medium-Range Weather Forecasts 40-year reanalysis (ERA-40). *J. Geophys. Res.* **109**, D18107, doi:10.1029/2004JD004816.

Barron, C. N. and Smedstad, L. F. 2002. Global river inflow within the Navy Coastal Ocean Model. Proc. Oceans 2002 MTS/IEEE Conference, 29–31 October, 1472–1479.

Barron, C. N. and Kara, A. B. 2006. Satellite-based daily SSTs over the global ocean. *Geophys. Res. Lett.* **33**, L15603, doi:10.1029/2006GL026356.

Behrenfeld, M. J., Randerson, J. T., McClain, C. R., Feldman, G. C., Los, S. O. and co-authors. 2001. Biospheric primary production during an ENSO transition. *Science* **291**, 2594–2597.

Bleck, R. 2002. An oceanic general circulation model framed in hybrid isopycnic-cartesian coordinates. *Ocean Modell.* **4**, 55–88.

Boyer, T. P., Antonov, J. I., Garcia, H. E., Johnson, D. R., Locarnini, R. A. and co-authors. 2006. *World Ocean Database 2005*, DVDs, *NOAA Atlas NESDIS*, Vol. 60 (ed. S. Levitus), NOAA, Silver Spring, MD, 190 pp.

Carnes, M. R. 2009. Description and evaluation of GDEM-V3.0. NRL Report NRL/MR/7330–09-9165. [Available from http://www7320.nrlssc.navy.mil/pubs.php.]

Casey, K. S. and Cornillon, P. 1999. A comparison of satellite and in situ based sea surface temperature climatologies. *J. Climate* **12**, 1848–1863.

Chassignet, E. P., Hurlburt, H. E., Metzger, E. J., Smedstad, O. M., Cummings, J. A. and co-authors. 2009. US GODAE global ocean prediction with the HYbrid Coordinate Ocean Model (HYCOM). *Oceanography* **22**, 64–75.

Enfield, D. B. 1996. Relationships of inter-American rainfall to tropical Atlantic and Pacific SST variability. *Geophys. Res. Lett.* **23**, 3305–3308.

Gibson, J. K., Kållberg, P., Uppala, S., Hernandez, A., Nomura, A. and co-authors. 1997. ECMWF Re-Analysis Project Report Series: 1. ERA description (Version 2), 74 pp.

Hanley, D. E., Bourassa, M. A., O'Brien, J. J., Smith, S. R. and Spade, E. R. 2003. A quantitative evaluation of ENSO indices. *J. Climate* **16**, 1249–1258.

Hurlburt, H. E., Chassignet, E. P., Cummings, J. A., Kara, A. B., Metzger, E. J. and co-authors. 2008. Eddy-resolving global ocean prediction. In: *Ocean Modeling in an Eddying Regime* (eds M. Hecht and H. Hasumi). *Geophys. Monograph* 177, 353-381. Amer. Geophys. Union, Washington, DC.

Kara, A. B. and Barron, C. N. 2007. Fine-resolution satellite-based daily sea surface temperatures over the global ocean. *J. Geophys. Res.* **112**, C05041, doi:10.1029/2006JC004021.

Kara, A. B., Rochford, P. A. and Hurlburt, H. E. 2000a. Efficient and accurate bulk parameterizations of air–sea fluxes for use in general circulation models. *J. Atmos. Oceanic Technol.* **17**, 1421–1438.

Kara, A. B., Rochford, P. A. and Hurlburt, H. E. 2000b. An optimal definition for ocean mixed layer depth. *J. Geophys. Res.* **105**, 16 803–16 821.

Kara, A. B., Wallcraft, A. J. and Hurlburt, H. E. 2003. Climatological SST and MLD simulations from NLOM with an embedded mixed layer. *J. Atmos. Oceanic Technol.* **20**, 1616–1632.

Kara, A. B., Wallcraft, A. J. and Hurlburt, H. E. 2005a. A new solar radiation penetration scheme for use in ocean mixed layer studies: an application to the Black Sea using a fine resolution HYbrid Coordinate Ocean Model (HYCOM). *J. Phys. Oceanogr.* **35**, 13–32.

Kara, A. B., Hurlburt, H. E., Wallcraft, A. J. and Bourassa, M. A. 2005b. Black Sea mixed layer sensitivity to various wind and thermal forcing products on climatological time scales. *J. Climate* **18**, 5266–5293.

Kara, A. B., Metzger, E. J., Hurlburt, H. E., Wallcraft, A. J. and Chassignet, E. P. 2008. Multistatistics metric evaluation of ocean general circulation model sea surface temperature: application to 0.08° Pacific Hybrid Coordinate Ocean Model simulations. *J. Geophys. Res.* **113**, C12018, doi:10.1029/2008JC004878.

Kara, A. B., Barron, C. N. and Boyer, T. P. 2009a. Evaluations of SST climatologies in the tropical Pacific Ocean. *J. Geophys. Res.* **114**, C02021, doi:10.1029/2008JC004909.

Kara, A. B., Wallcraft, A. J., Hurlburt, H. E. and Loh, W.-Y. 2009b. Which surface atmospheric variable drives the seasonal cycle of sea surface temperature over the global ocean? *J. Geophys. Res.* **114**, D05101, doi:10.1029/2008JD010420.

Kara, A. B., Wallcraft, A. J., Hurlburt, H. E. and Loh, W.-Y. 2009c. Quantifying SST errors from an OGCM in relation to atmospheric forcing variables, *Ocean Modell.* **29**, 43–57.

Large, W. G., McWilliams, J. C. and Doney, S. C. 1994. Oceanic vertical mixing: a review and a model with a nonlocal boundary layer parameterization. *Rev. Geophys.* **32**, 363–403.

Lau, K. M., Wu, H. T. and Bony, S. 1997. The role of large scale atmospheric circulation in the relationship between tropical convection and sea surface temperature. *J. Climate* **10**, 381–392.

Locarnini, R. A., Mishonov, A. V., Antonov, J. I., Boyer, T. P. and Garcia, H. E. 2005. *World Ocean Atlas 2005*, vol. 1, *Temperature*, edited by S. Levitus, *NOAA Atlas NESDIS 61*, 182 pp., U.S. Government Printing Office, Washington, DC.

McPhaden, M. J. 1999. Genesis and evolution of the 1997-98 El Niño. *Science* **283**, 950–954.

Mitchell, T. P. and Wallace, J. M. 1992. The annual cycle in equatorial convection and sea surface temperature. *J. Climate* **5**, 1140–1156.

Murphy, A. H. 1995. The coefficients of correlation and determination as measures of performance in forecast verification. *Wea. Forecast.* **10**, 681–688.

Nagura, M., Ando, K. and Mizuna, K. 2008. Pausing the ENSO cycle: a case study from 1998 to 2002. *J. Climate* **21**, 342–363.

Nakajima, K., Toyodo, E., Ishiwatari, M., Takehiro, S.-I. and Hayashi, Y.-Y. 2004. Initial development of tropical precipitation patterns in response to a local warm SST area: an aqua-planet ensemble study. *J. Meteor. Soc. Japan* **82**, 1483–1504.

Perry, G. D., Duffy, P. B. and Miller, N. L. 1996. An extended data set of river discharges for validation of general circulation models. *J. Geophys. Res.* **101**, 21 339–21 349.

Reynolds, R. W., Rayner, N. A., Smith, T. M. and Stokes, D. C. 2002. An improved in-situ and satellite SST analysis for climate. *J. Climate* **15**, 1609–1625.

Smith, W. H. F. and Sandwell, D. T. 1997. Global sea floor topography from satellite altimetry and ship depth soundings. *Science* **277**, 1956–1962.

Wallcraft, A. J., Kara, A. B., Hurlburt, H. E. and Rochford, P. A. 2003. The NRL Layered Global Ocean Model (NLOM) with an embedded mixed layer submodel: formulation and tuning. *J. Atmos. Oceanic Technol.* **20**, 1601–1615.